HOSTED BY
ELSEVIER
CrossMark
Available online at www.sciencedirect.com
ScienceDirect
Biosurface and Biotribology 2 (2016) 26–39
www.elsevier.com/locate/bsbt

A functional effect of the superficial mechanical properties of articular cartilage as a load bearing system in a sliding condition

N. Sakai[a,c,*], C. Hashimoto[a], S. Yarimitsu[b], Y. Sawae[a,c], M. Komori[a], T. Murakami[c]

[a]*Integrated System Engineering, Kyushu Institute of Technology, Kitakyushu, Japan*
[b]*Intelligent Mechanical Systems, System Design, Tokyo Metropolitan University, Tokyo, Japan*
[c]*Research Center for Advanced Biomechanics, Kyushu University, Fukuoka, Japan*

Received 20 November 2015; received in revised form 21 February 2016; accepted 22 February 2016

Abstract

The structure and composition of articular cartilage show depth-wise inhomogeneity and anisotropy. In particular, the dense collagen network covers and reinforces the superficial tangential zone of the tissue. It is thought that this peculiar structure offers the excellent tribological property of articular cartilage. The purpose of this study was to investigate the functionality of the superficial tangential zone (STZ) of articular cartilage as a load bearing system. The 2-dimensional finite element (FE) model was accepted for sliding configuration with sufficient extent of sliding distance. The standard model as a control was carried from our previous study, which included depth-dependent Young's modulus of the solid phase, fiber reinforcement with strain-dependency and permeability with compaction effect. The mechanical property of the superficial layer was modified for a parametric study of its functionality. According to research results in the past, the tangential stiffness of the fiber reinforcement of the STZ model was enhanced, and the following anisotropic permeability was also modified. The stationary contact condition and the migrating contact condition were examined to compare the effect of the superficial tangential layer. The result showed that the significant reduction of friction coefficient was found in migrating contact condition of the STZ model. In the observation of field output of FE analysis, the contacting surface formed a thin low permeability layer, which would enable the high fluid pressure and the low fluid flow at the same time. It seemed that the stiffening of the fiber reinforcement of the superficial layer promoted the formation of the low permeability layer. Beyond the effectivity of the fiber reinforcement of biphasic matrix on the interstitial fluid pressurization, the findings of this study indicated that the compaction effect on the permeability would involve a quite complex phenomenon in long term migrating contact sliding.
© 2016 Southwest Jiaotong University. Production and hosting by Elsevier B.V. This is an open access article under the CC BY-NC-ND license (http://creativecommons.org/licenses/by-nc-nd/4.0/).

Keywords: Articular cartilage; Biphasic lubrication; Load bearing; Material property; Anisotropy; Inhomogeneity

1. Introduction

Articular cartilage plays an important role to maintain very low friction in wide operating ranges. The study on the mechanics of the cartilaginous tissue is usefully applicable to a medical insight of the synovial joint diseases, cultivating conditions for regenerative medicine and an engineering feature of a load bearing system such as artificial cartilage. The cartilaginous tissue contains high water fraction as a fluid phase. Proteoglycan matrix is enmeshed in type II collagen fibril network, which mainly resists the tensile load. The cartilaginous tissue is commonly divided into 3 characteristic layers, whose are called superficial, middle and deep zone. In the superficial zone, the constitution of collagen fibril network is dense and predominantly oriented to parallel with tissue surface [1–3]. Articular cartilage shows compressive strain inhomogeneity and anisotropy from the surface to deep zone [4–7]. The tensile stiffness of cartilaginous tissue is experimentally much higher than the compressive stiffness in equilibrium condition [8], and mechanical behavior of articular cartilage tissue exhibits tension–compression nonlinearity [9].

*Corresponding author at: Integrated System Engineering, Kyushu Institute of Technology, Kitakyushu, Japan. Tel./fax: +81 93 884 3574.
E-mail address: sakai.nobuo@ise.kyutech.ac.jp (N. Sakai).
Peer review under responsibility of Southwest Jiaotong University.

http://dx.doi.org/10.1016/j.bsbt.2016.02.004
2405-4518/© 2016 Southwest Jiaotong University. Production and hosting by Elsevier B.V. This is an open access article under the CC BY-NC-ND license (http://creativecommons.org/licenses/by-nc-nd/4.0/).

Articular cartilage realizes excellent frictional property by the synergistic cooperation of several frictional modes, called as "adaptive multimode lubrication" [10]. At low sliding speed, several boundary lubrication mechanisms considerably enhance the tribological property [11–19]. Articular cartilage shows the time-dependent compressive behavior, which was well explained by "biphasic model" [20]. The further biphasic complex of articular cartilage on frictional behavior has been expanded as "biphasic lubrication mechanism" [21]. When an impermeable counter surface contacts to the biphasic material, the interstitial fluid is trapped and pressurized within the apparent contact area. While the fluid starts flowing along the gradient of the pressure, the pressurized interstitial fluid also presses the solid phase, which is well reinforced in the tensile direction by the collagen network. This situation causes high fluid pressurization in the contact area and the consequent reduction of the solid-to-solid contact load. The high fluid load support results in low friction coefficient under an assumption of a nonviscous property of the fluid [22]. As the fluid load pressurization was observed in unconfined compression [23], the reduction of friction coefficient was experimentally proved by the correlation between the direct measurement of the contact fluid pressure and friction coefficient [24].

It is said that excessive loading cycles increase the possibility of the disruption of the collagen–proteoglycan construction [25]. The repeated compressive load of in-vitro study caused the reduction of tensile strength prior to the obvious surface damage [26]. In addition to the mechanical weakening, the fragments of collagen II and glycosaminoglycans were released to culture medium [27]. Semi-impact loading test also showed superficial disruption with textual alteration, whereas the deeper zone remained undamaged [28]. An anatomical observation following an indentation test showed the structure-related deformation associated with the superficial tangential zone [29]. The removal of the superficial zone completely changed the typical deformation field of the indentation test [30,31]. Once a splitting of the cartilage surface occurs eventually, the surface lesion develops into full thickness of the cartilaginous tissue with surface roughening and fibrillation. The surface structure with the fiber reinforcement is thought to be an important factor for the functionalities of articular cartilage.

A computational model indicated that the experimental indentation well correlated with the stiffness of superficial layer [32]. The tensile stiffness of the thin specimen including superficial layer was about 6 times higher than that prepared from the middle layer [33]. Because of the difficulties of the experimental testing, prescribed FE model and curve fitting method were utilized to estimate the material properties including the inhomogeneity and the anisotropy. The orientation and the density of collagen network for FE model were determined by microstructural insights [34,35], and verified by quantitative optical analysis [36]. In addition to the material testing, the depth-dependent inhomogeneity enhanced the ratio of the interstitial fluid support in spherical indentation [37].

Anisotropy of fluid transport was evaluated in the past by diffusional anisotropy using fluorescence recovery after photobleaching (FRAP). In the superficial layer, macromolecular diffusion showed significant anisotropic property in particularly the compressed condition [38], in which the diffusion rate in the fiber direction was larger than perpendicular direction. On the other hand, the curve fitting estimation in compressed condition showed a significant decrease of the permeability perpendicular to the compression [39]. Since the anisotropy of the permeability was thought to derive from an intrinsic structural mechanism of the fiber arrangement, the depth-dependent anisotropy of the permeability was estimated by the curve fitting method of FE analysis using the prescribed distribution of the density and the orientation of collagen fiber network [40].

A knee model with the depth-dependent anisotropy enhanced the fluid load support in a loading condition [41]. Beyond the loading analysis, the migrating sliding configuration as a start-up friction was examined to confirm the effect of anisotropic low tangential permeability in the superficial layer [42], which resulted in a reduction of friction coefficient. For the biphasic lubrication mechanism, the tensile reinforcement of the tissue by the collagen network plays a crucial role to enhance the interstitial fluid pressurization and for following superior frictional property. The superficial tangential layer is reinforced with the dense collagen network This structure is interesting from not only a physiological viewpoint but also an engineering viewpoint as a load bearing system. In the present study, we focused on the effect of anisotropic fiber reinforcement in the superficial tangential zone, which also involved anisotropic permeability property. The transitional friction coefficient in sliding condition was examined using biphasic FE analysis. The result showed that a peculiar decrease of friction coefficient was observed in migrating contact condition.

2. Materials and method

In this study, we firstly prepared a standard biphasic FE model as a control model. Although the material properties of the standard model were carried from our previous paper [43], we summarize the composition of the standard model according to the purpose of this study. Then, the material properties of the superficial tangential layer of the standard model were altered to assess the effect of anisotropic material properties from an engineering viewpoint. The effect of the anisotropic superficial layer was evaluated by 2 sliding conditions, which were the cylindrical cartilage sliding on a plate and the cylindrical indenter sliding on the cartilage. The latter sliding condition was the migrating contact condition as a dynamic condition, which was introduced in the papers past [44,45]. Several parametric studies beyond the biological condition were also conducted for confirming the effect and further applications.

2.1. The constitution of the standard model

A commercial package for FE analysis (ABAQUS Ver.6.8-4) was used in this study. The 2-dimentional modeling was

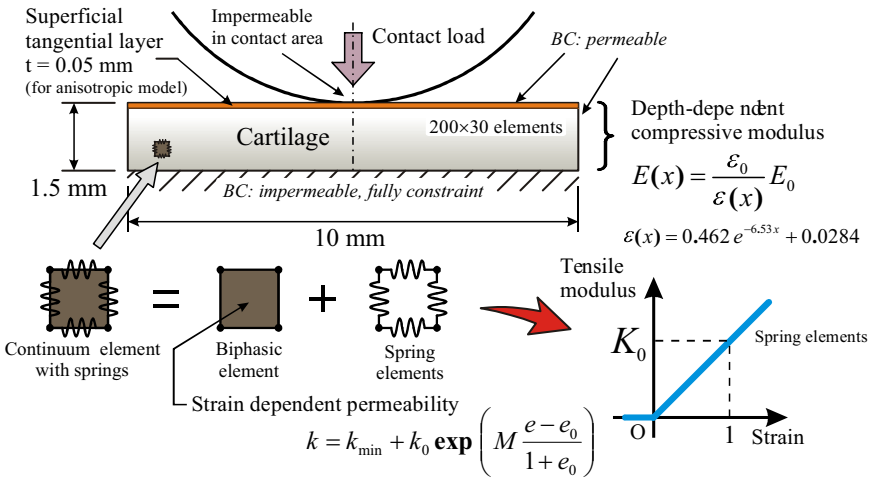

Fig. 1. Schematic drawing of the cartilage model. The finite element model included depth-dependent compressive modulus, collagen network reinforcement with strain-dependent tensile modulus and strain-dependent permeability. For the anisotropic model, spring reinforcement in the tangential direction and following permeability of the superficial tangential layer were modified with the respective to specified conditions.

admitted for saving computational time and for an unproblematic implementation of the sliding conditions. A schematic drawing of the cartilage model was shown in Fig. 1. The dimension of the FE model was 1.5 mm thickness and 10 mm length, which was the same dimensions in which the material properties were estimated by cylindrical indentation [43]. The biphasic matrix was modeled by CPE4RP (four-node bilinear displacement and pore pressure, reduced integration with hourglass control, plane strain-based element) elements with 0.05 mm^2 size. The total biphasic elements in the model were summed up to 200×30 elements. The bottom of the matrix was impermeable and fully constraint. The other surfaces were not fixed and permeable except for the contact surface. The surface seepage in the contact area was controlled by a user subroutine, in which the FLOW function regulated the surface seepage coefficient as zero in the contact area. In the other non-contact surface, the surface seepage coefficient was set to one as a sufficiently large value [44]. We thought that the depth-dependency as an inhomogeneity of the tissue was the important factor to improve frictional property [37,45]. By a video microscopic observation during a definite compression test, the depth-dependent local strain $\varepsilon(x)$ as the inhomogeneity along the depth was experimentally obtained in an equilibrium condition [46] as the function of relative position x ($0 < x < 1$; normalized position $x = 0$ means the surface position) by

$$\varepsilon(x) = 0.462e^{-6.53x} + 0.0284. \quad (1)$$

Using this equation, the depth-dependent Young's modulus $E(x)$ of the solid phase could be determined by an assumptive relationship between the total stress and the local stress as $E_0\varepsilon_0 = E(x)\varepsilon(x)$ in an equilibrium condition, in which the total strain ε_0 derived from the depth-integration of Eq. (1) and the total or apparent Young's modulus E_0 was estimated by the curve fitting method using FE analysis. The effect of biphasic surface amorphous layer [47,48] would be partly included by the enough small value of the Young's modulus $E(0)$ through the tissue depth. Poisson's ratio of the solid phase was set to 0.125 as a typical value since the small value of Poisson's ratio has been accepted and estimated in the past [6,34–36,43–48]. For the interstitial fluid flow, the permeability showed a strong dependency on the strain of the solid phase. In this study, the relationship between the strain of the solid phase ε and the permeability k was defined by

$$k = k_{min} + k_0 \exp[M\varepsilon], \quad (2)$$

where k_0 is the base permeability on the strain dependency, M represents the effectiveness of the compaction effect [49]. The lower limit of the permeability k_{min} was introduced for an acceptable curve fitting result of FE analysis in seeking material properties [6]. The supplement of k_{min} was also effective for the reproducibility of a creep behavior in cylindrical indentation [43]. The strain of the solid phase ε in Eq. (1) was written with the initial void ratio e_0 and the current void ratio e by $\varepsilon = (e - e_0)/(1 + e_0)$. The initial void ratio ε_0 is a constant value and was set to 4.0 as the typical one, which means the volumetric proportion of the interstitial fluid is 80%. It was thought that the reinforcement of the collagen network in articular cartilage well enhanced the interstitial fluid pressure. The deep vertical collagen fibril also promoted interstitial fluid pressurization in a dynamic cylindrical indentation [50]. The fiber reinforcement of the standard model in this study was homogenous and isotropic in horizontally and vertically directions as an orthogonal manner, which were modeled by spring element SPRINGA (axial spring between two nodes, whose line of action is the line joining the two nodes) of the software package. The spring element was configured to resist in only tensile direction. It was reported that both of the strain-dependent permeability as the compaction effect and the non-linear fibril reinforcement were required to represent the compressive response and the creep response by single parameters set simultaneously [51]. The apparent stress component by the spring reinforcement σ_{sp} was written by $\sigma_{sp} = K(\varepsilon)\varepsilon$, where the incremental stiffness modulus $K(\varepsilon)$ was the function of ε. In this study, we assumed

Table 1
Material properties of articular cartilage for the standard model. The values with asterisk mark (*) were estimated by the curve fittings of the finite element analysis [43].

Parameter	Value
Young's modulus (E_0)*	0.83 MPa
Depth-dependent strain in equilibrium ($\varepsilon(x)$)	$0.462e^{-6.53x}+0.0284$
Poisson's ratio	0.125
Lower limit of permeability (k_{min})*	5.0×10^{-15} m^4/N s
Base of strain dependent permeability (k_0)*	58.86×10^{-15} m^4/N s
Compaction effect on permeability (M)*	22
Initial void ratio (e_0)	4.0 (80% interstitial fluid)
Spring stiffness component (K_0)*	17.5 MPa
Seepage coefficient	1 mm^3/N s in flowing condition 0 mm^3/N s in contact condition
Friction coefficient between solid-to-solid (μ_{eq})	0.2

that the modulus $K(\varepsilon)$ was the linear function of the strain ε, as written by $K(\varepsilon)=K_0\varepsilon$. The spring stiffness component K_0 was referred from the our previous study. Using these equation, the spring stiffness of each SPRINGA element was respectively determined by the spring density and the spring length, namely the mesh size. The material properties for the standard model were shown in Table 1 [43].

2.2. Inhomogenous and anisotropic material properties of the superficial tangential layer

The purpose of this study is to ascertain the functional effect of anisotropic mechanical properties of the superficial tangential layer as a load bearing system in sliding condition. From both an engineering viewpoint and the parametric study, the mechanical properties of the superficial layer of the standard model were simply modified to anisotropic one. The modified parameters were the stiffness of fiber reinforcement and the permeability following the fiber. In the past, the tensile stiffness of superficial tangential layer of articular cartilage was directry measured by an experimental tensile test. However, the tangential thin specimen sliced from middle and deep zone did not keep its shape and could not be fixed to the clamps [33]. Meanwhile, with the experimental difficulty, several reports attempted to estimate the material properties of superficial tangential layer by the microstructual construction [34,35]. They firstly defined the collagen density and the primary direction of the collagen network by the microstructural insights. Then, the prescribed structure was implemented in the FE model, and was used to estimated the anisotropic tensile stiffness of the superficial layer by the curve fitting method. Wilson et al. [34] reported that the density of the primary orienting collagen relative to the secondary random one was 3.74. So, we borrowed the value 3.74 as the stiffness anisotropy of the tangential direction in superficial layer. For the anisotropic model in this study, the horizontal stiffness of the superficial spring elements was modified 4.74 times larger value than the homogenous randam stiffness of the standard model. The anisotropy of the fluid transport in the fibrillar tissue was often observed by the diffusional behavior using fluorescence recovery after photobleaching [52] or recent magnetic resonance imaging [53]. As reported by Fujie et al. [42], the decrease in tangential permeability of superficial tangential layer resulted in a positive effect on the frictional property. On the other hand, several studies reported the increase of the permeability along fiber direction [52,53], which might cause a little negative effect in the superficial tangential layer. Meanwhile, the fiber reinforcement would show a possible positive effect on frictional behavior. To compare the positive effect of the fiber reinforcement with the negative effect of the increased tangential permeability, we accepted the increase of the permeability caused by the fiber reinforcement as a worse case. Although it was estimated that the anisotropic permeability was not so significant in comparison with the fibrillar property [54], Federico and Herzog implemented the anisotropy of permeability by considering the microstructural arrangement of the collagen fibrils [40] under an assumption that the collagen fiber is impermeable and obstructs the interstitial fluid flow. In their calculation, the tangential permeability in the superficial layer was 1.090 times larger than that of the random fibrillar zone. The vertical permeability in the superficial layer was also estimated as 0.818 times, in which the ratios of the permeability was predicted in the volumetric fraction of the collagen fiber being 0.4 as a typical value in the superficial layer. Using these values, the permeability of the anisotropic model was modified with the respective direction as proposed in the past [55]. In this study, the same material parameter M of the standard model was used for the anisotropic model in tangential and perpendicular direction. In the following parametric study, the material properties were proportionally modified with the respective magnitude of value change. The modified material properties for the superficial tangential layer was summarized in Table 2.

Table 2
Material properties of the superficial tangential layer for the anisotropic model. The spring stiffness in tangential direction was 4.74 times larger value than that of random collagen region. The permeability in the perpendicular direction was reduced to 0.818 times value. The permeability in the tangential direction was 1.090 times larger value than the random one.

Parameter	Value
Spring stiffness component in the perpendicular ($K_{0\perp}$)	17.5 MPa
Spring stiffness component in the tangential ($K_{0=}$)	82.95 MPa
Lower limit of permeability in the perpendicular ($k_{min\ \perp}$)	4.09×10^{-15} m^4/N s
Base permeability in the perpendicular ($k_{0\perp}$)	48.15×10^{-15} m^4/N s
Lower limit of permeability in the tangential ($k_{min\ =}$)	5.45×10^{-15} m^4/N s
Base permeability in the tangential ($k_{0=}$)	64.16×10^{-15} m^4/N s

2.3. Sliding analysis

The sliding analysis was performed using the prescribed models in 2 different sliding condition, as shown in Fig. 2. One of the conditions was the cartilage indenter with 5 mm radius at the surface sliding over an impermeable plate as a stationary contact condition. The other sliding condition was the impermeable cylindrical indenter with 5 mm radius sliding over the tissue plate as a migrating contact condition [44,45]. In both of the sliding condition, the contact force of 0.5 N/mm

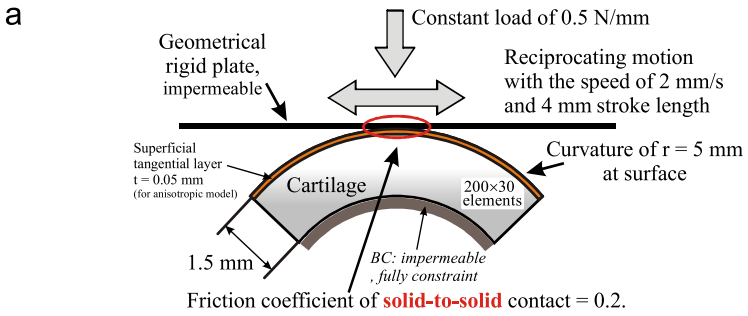

The cartilage indenter with 5 mm radius at the surface sliding over an impermeable plate as a stationary contact condition.

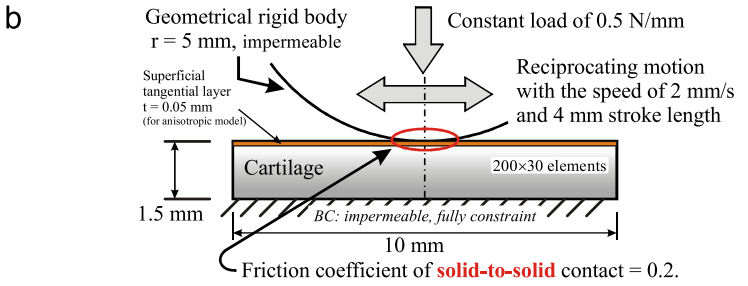

The impermeable cylindrical indenter with 5 mm radius sliding over the tissue plate as a migrating contact condition.

Fig. 2. The sliding conditions for frictional analysis. The stationary contact condition (a) and the migrating contact condition (b) were examined as an experimental load bearing condition.

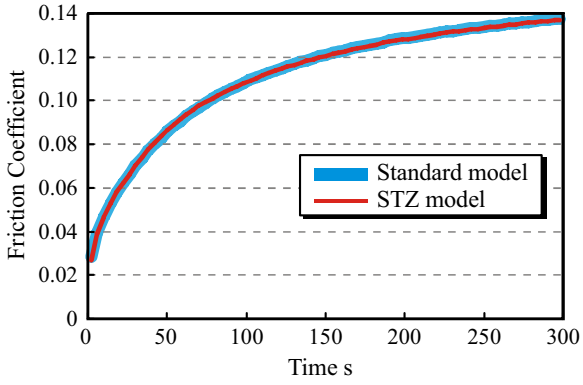

Fig. 3. Transient of friction coefficient of the stationary contact condition. "STZ model" represents the model in which the stiffness of the fiber reinforcement was modified 4.74 times and the following permeability was also changed.

was loaded with a ramp profile through 1 second before starting sliding. In this loading, the contact length of the stationary contact condition and the migrating contact condition just after starting sliding were about 2.3 and 2.1 mm, respectively. While the normal load was kept, the indenter slid reciprocally over the counter plate with the stroke length of 4 mm at the speed of 2 mm/s, in which one stroke took 4 s. The sliding motion lasted 300 s and was summed up to 75 cycles. The friction coefficient between the impermeable plate/cylinder and the solid phase of the biphasic cartilage surface μ_{eq} was set to 0.2 as a typical value of an experimental sliding test in the condition that the boundary lubrication mechanism does not work enough. The time course of friction coefficient was averaged in 90% of the single directional path of the reciprocal motion, so the data around 0.1 s of the directional change in the reciprocal motion was excluded from the calculation of frictional coefficient. At typical time periods, the proportion of the fluid load support was calculated in the contact length. The threshold for limiting the change of the interstitial fluid pressure in a single time integration was specified of 0.05 kPa by UTOL parameter for transient analysis, which regulated the time integration length within about 0.03 s through the calculation.

3. Results

Transient of friction coefficient in the cylindrical cartilage indenter sliding over the impermeable plate was shown in Fig. 3. In figures, the "STZ model" represents the model in which the stiffness of the fiber reinforcement was modified 4.74 times and the following permeability was also changed, shown in Table 2. In the stationary contact condition, the difference of the transient friction coefficient between the standard model and STZ model was very little. The other conditions in the parametric study, whose were not shown in this report, also showed only small differences within our parameters in comparison with the following migrating contact condition. On the other hand, the sliding condition of the migrating contact condition showed the interesting transition of friction coefficient, as shown in Fig. 4. The difference of the friction coefficient was not so large at the beginning of the sliding, in which the friction coefficient of the STZ model was a little smaller than that of the standard model. However, the difference gradually enlarged with time progress. The standard model increased friction coefficient more than 0.04,

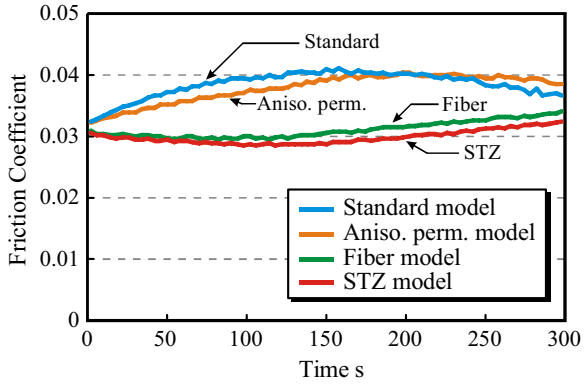

Fig. 4. The sliding condition of the migrating contact condition. The standard model increased friction coefficient more than 0.04, whereas the STZ model decreased it less than 0.03 after 100 s sliding. The anisotropic permeability in itself showed an admittable reduction of friction coefficient. The strengthening of fiber reinforcement in the tangential direction in the superficial layer showed significant reduction of friction coefficient.

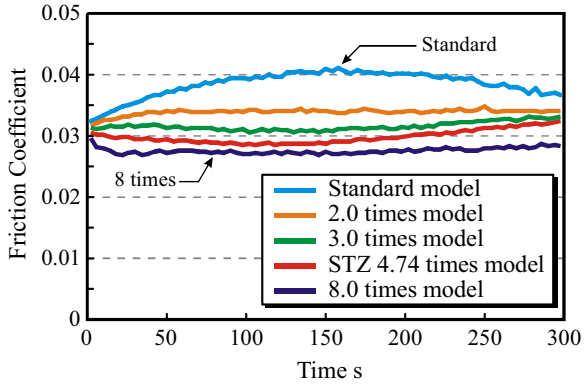

Fig. 5. The effectiveness on the strengthening of the tangential stiffness of the collagen in the superficial layer. "STZ 4.74 times model" is as the same data as "STZ model" in Fig. 4. The more strengthening of the tangential collagen resulted in the less friction coefficient.

whereas the STZ model decreased it less than 0.03 after 100 s sliding. Since the STZ model was modified both the stiffness of collagen reinforcement and the permeability simultaneously, we checked which parameter was effective for this phenomenon. In the Fig. 4, the "Aniso. perm. model" included only the modification of the permeability in Table 2. Meanwhile, the "Fiber model" was modified only the stiffness of the collagen reinforcement. The friction coefficient of the anisotropic permeability model, "Aniso. perm. model", showed an admittable reduction of the friction coefficient in the first half of the continuous sliding. Whereas the effect of the anisotropic permeability was not a negligible thing, the "Fiber model" showed the significant decrease of the friction coefficient over the whole sliding term. Additional reduction of the friction coefficient was observed in the STZ model, which included all modification shown in Table 2. We could see that the increased stiffness of collagen reinforcement in the tangential direction and following change of the permeability were both effective for the migrating contact condition, and did not hinder the effect mutually. The further parametric study was conducted to determine the effect of STZ modification. Fig. 5 shows the effectiveness on the strengthening of the tangential stiffness of the collagen in the superficial layer. The "STZ 4.74 times model" in Fig. 5 is as the same plot as the "STZ model" in Fig. 4. For example, the "3.0 times model" represents the model which was increased the collagen stiffness in 3 times larger value, as $K_{0=} = 52.5$ MPa. In the "3.0 times model", the parameters on the base permeability $k_{0\perp}$ and $k_{0=}$ were also modified with the values of 53.13×10^{-15} and 61.69×10^{-15} m^4/Ns respectively, in which the value changes from the standard model were smaller than those of The "STZ 4.74 times model". As the strengthening of the collagen reinforcement developed, the friction coefficient totally reduced over whole the sliding time. The extra attempt for the strengthening of the collagen stiffness by 8.0 times showed the further decrease of the friction coefficient and maintained it in a long time until the sliding end of 300 s. The more strengthening of the tangential collagen resulted in the less friction coefficient.

To confirm the transition of friction coefficient, we moved to check the proportion of the fluid load support in parallel with the loading direction. Fig. 6 shows the proportion in stationary contact condition, as the friction coefficient was shown in Fig. 3. In the FE analysis in this study, the friction coefficient deriving from the horizontal fraction of the surface traction was simply governed by the equilibrium solid-to-solid friction coefficient μ_{eq} and the proportion of the load partitioning by the solid phase. For example, the friction coefficient of the standard model in stationary contact condition at 100 s was calculated by $\mu_{eq} \times 54.3\% = 0.109$, which could be read as almost the same value in Fig. 3. The fluid load support of the STZ model at 0 s, which means the time immediately after the completion of the contact load exertion, was smaller than that of the standard model in Fig. 6. The fluid load support at 0 s of the stationary contact condition is thought to relate the startup friction or the static friction. The proportion of the fluid load support in the migrating contact condition is shown in Fig. 7. The fluid load support in this study meant that the parallel fraction of the fluid contact pressure with the 0.5 N loading direction, as shown in Fig. 2(b). So, the friction coefficient in the migrating contact condition included both the traction of the solid-to-solid contact and the plowing friction. For example, the friction coefficient of the STZ model in migrating contact condition at 100 s was calculated as 0.027 from the proportion of the fluid load support as the frictional fraction deriving from the solid-to-solid traction. The remainder was thought to be the friction by the plowing mechanism. The proportion of the fluid load support of the anisotropic surface models showed the smaller value than that of the standard model. While the fluid load support of the "STZ 4.74 times model" gradually decreased with the sliding time passing, the "8.0 times model" as an extra parametric study maintained the proportion of the fluid load support within 12.5% until 300 s.

In this situation, we had to observe the internal behavior of the cartilage model. Fig. 8 shows Mises stress field of the standard model and the STZ model around the indenter at 100 s in the migrating contact condition. At the time, the cylindrical indenter was moving in the right direction. It was notable that the Mises stress of the superficial thin layer under the indenter formed a low-stress layer in the STZ model. In other words, the

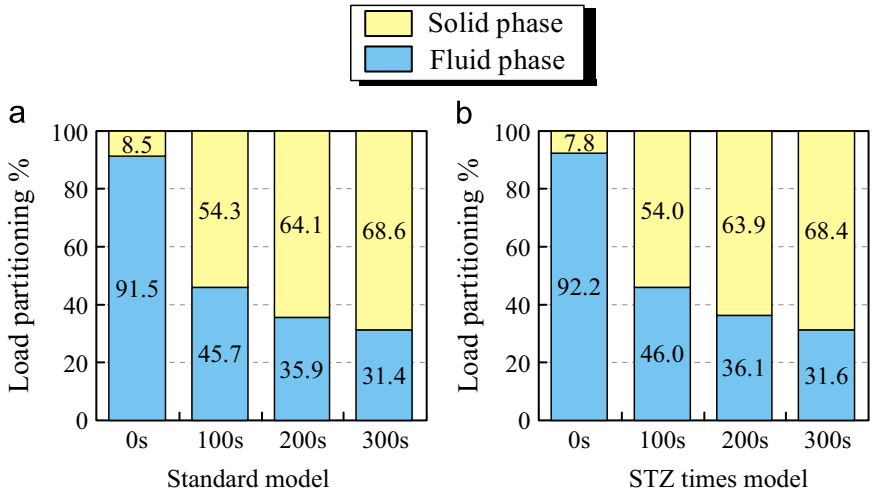

Fig. 6. The transition of the load partitioning between the solid and fluid phase at the contact area in the stationary contact condition. The friction coefficient in the stationary contact condition could be calculated by the equilibrium solid-to-solid friction coefficient and the proportion of the load partitioning of the solid phase.

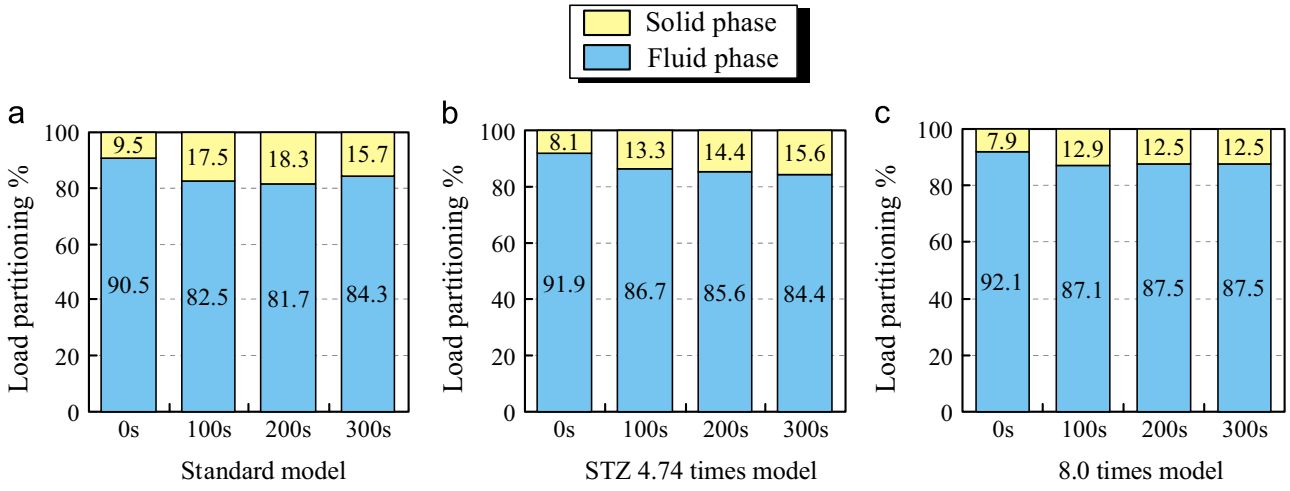

Fig. 7. The transition of the load partitioning between the solid and fluid phase at the contact area in the migrating contact condition. While the fluid load support of the "STZ 4.74 times model" gradually decreased with the sliding time passing, the "8.0 times model" as an extra parametric study maintained the proportion of the fluid load support until 300 s.

proportion of the fluid pressure at the surface should be higher in the STZ model because of the constant total load of 0.5 N. The distribution of the pore pressure is shown in Fig. 9, in which the scale was as same as that of Mises stress. The length of the high pore pressure region in the STZ model was a little wider than that of the standard model in the superficial layer. Since the superficial fiber reinforcement of the STZ model was specially stiffened by 4.74 times than that of the standard model, the STZ model generated the negative pressure region in front of the indenter sliding the right direction. The negative pressure of the superficial layer would be effective for the re-swelling process from the surface. Next, we observed the flow velocity vector of the interstitial fluid in Fig. 10. The flow velocity in the superficial layer in the STZ model was smaller than that of the standard model, especially in the frontal contact zone, whereas the pressure gradient as seen in Fig. 9 did not show an apparent difference between the models. The trend of the flow direction in the STZ model was perpendicular to the surface rather than the tangential as shown in the standard model. Note that the tangential permeability in the STZ model was the larger value than the vertical value, listed in Table 2. The other field data for investigating this situation was the fluid volumetric proportion to the total volume of an element, as shown in Fig. 11, in which the fluid velocity vector was again superimposed to check the relationship between them. The initial volumetric proportion of the fluid phase was set to 0.8, as shown in Table 1 with the initial void ratio e_0. We found that the fluid proportion in the superficial layer of the STZ model decreased to near 71%, while that of the standard model remained in 77% in the contact zone. The reduction of the fluid proportion means the considerable reduction of the permeability.

4. Discussion

In this study, the effect of the strengthening of the tangential fiber reinforcement and the following modification of the permeability was examined mainly on the transient behavior of friction coefficient in sliding conditions. While the 2-dimentional

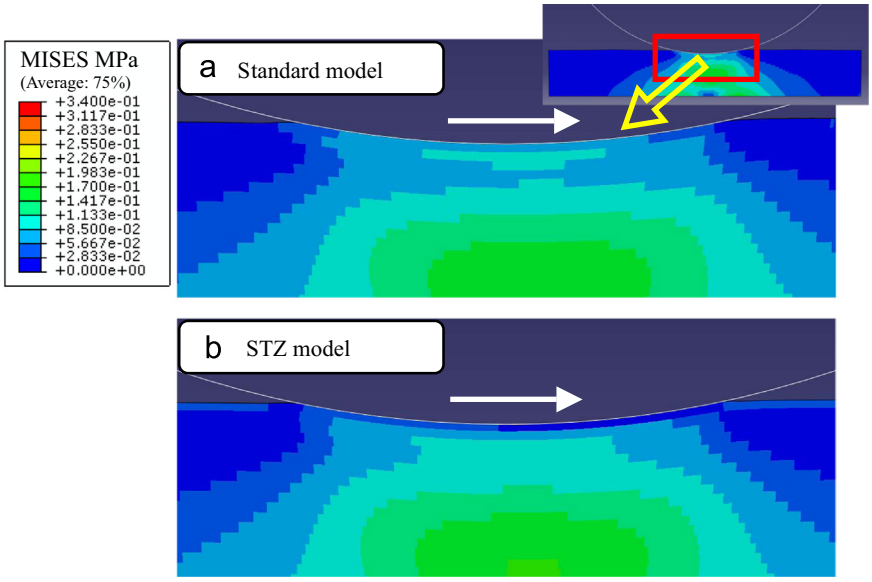

Fig. 8. Mises stress field of the standard model and the STZ model around the indenter at 100 s. The cylindrical indenter is moving in the right direction. These plots were the macrograph of the total model shown in the upper right figure. The superficial layer under the indenter formed a low-stress layer regarding Mises stress in the STZ model.

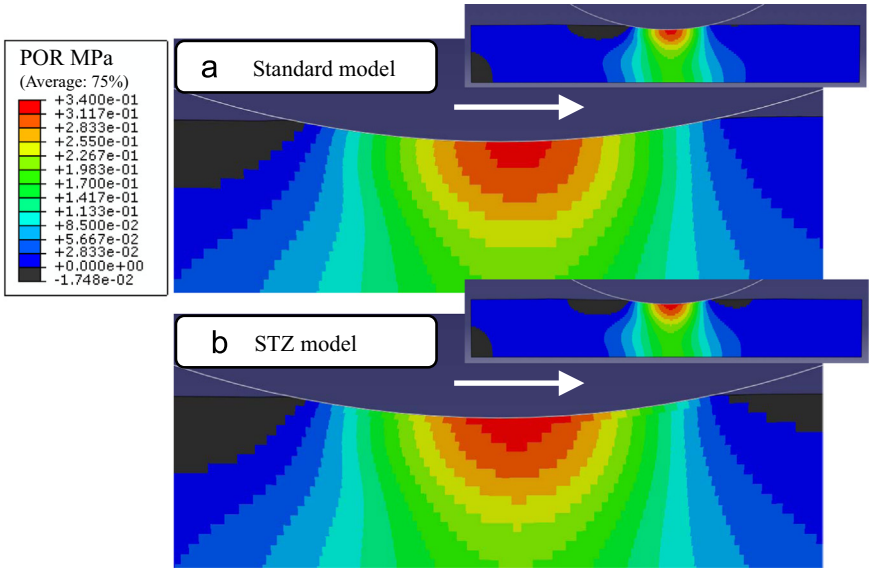

Fig. 9. The distribution of the pore pressure at 100 s. The STZ model generated the negative pressure region in front of the indenter sliding the right direction.

configuration was admitted for the incorporation of sliding motion, the standard model as a control model included depth-dependent Young's modulus of the solid phase, strain-dependent fiber reinforcement, and strain-dependent permeability as the compaction effect. In the stationary contact condition shown in Fig. 2(a), the tissue was thought to be exposed to a quasi-creep compressive condition. As Li et al. indicated in the past [51], those parameters could represent both the compressive behaviors and the creep behavior simultaneously [43]. Utilizing the standard model, the STZ model was built by simply modifying the material parameters of the superficial layer in the standard model. Although the modification of the standard model would mean that the model could not reproduce the accurate behavior of its original response, we decided to accept this methodology from an engineering viewpoint and further parametric studies. It is well known that the collagen network in the superficial layer predominantly oriented to the tangential direction. Because of the difficulty of the direct measurement of the anisotropic tensile modulus of articular cartilage, prescribed fields for the collagen density and orientation deriving from microscopic and constituent analyses were employed to estimate the material property of an FE model in the past [34,35]. Since the direct experimental measurement of the anisotropic permeability of articular cartilage also involved technical difficulties, Federico et al. proposed the collagen structure-related drag of the interstitial fluid flow for the estimation of the anisotropic permeability [40], which was

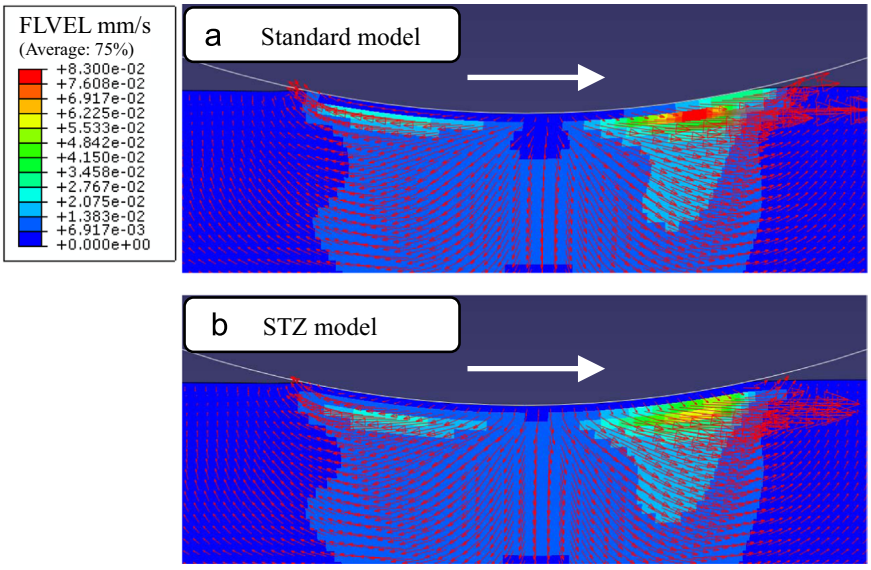

Fig. 10. The flow velocity and vector of the interstitial fluid at 100 s. The trend of the flow direction in the STZ model was perpendicular to the surface rather than the tangential shown in the standard model.

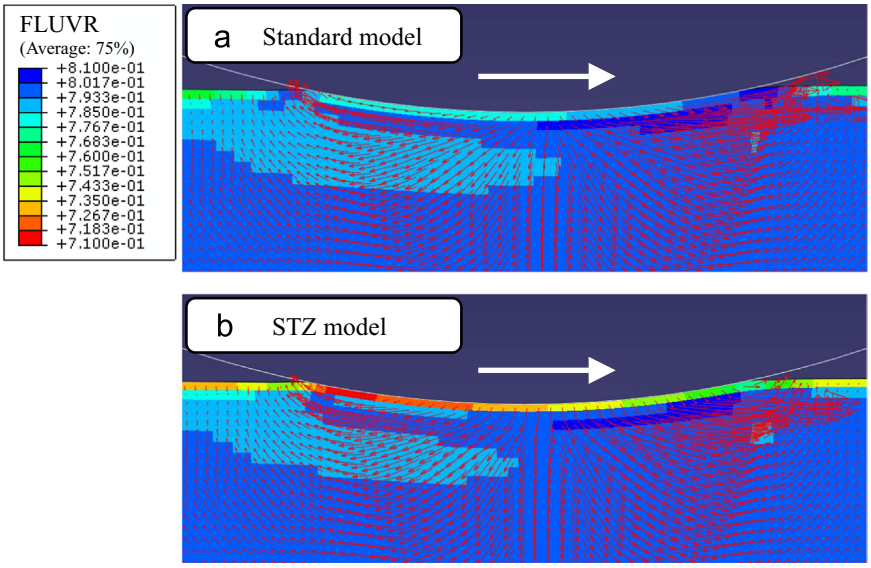

Fig. 11. The volumetric proportion of the fluid phase to the total volume of the element at 100 s. The fluid velocity vector was again superimposed in the plots. The fluid volume in the superficial layer was considerably decreased in the STZ model.

generalized to composite materials [56]. By the limitation of the experimental result for the superficial tangential layer, the estimated anisotropic material properties were adopted as typical values in this study. The standard model and the STZ model were examined to the stationary contact condition as a static condition and the migrating contact condition as a dynamic condition.

In the stationary contact condition, the difference between the models was not observed not only the transient of friction coefficient but also the internal field outputs, which were not presented in this paper. The fluid fraction of the contact center in the superficial layer in Fig. 2(a) almost squeezed out into the beneath layer before 84.1 s in the standard model and before 90.0 s in the STZ model respectively. This situation might be apparent because the compressive modulus of the surface was much smaller than that of the deeper zone, by the Eq. (1). Although the flowing out of the fluid fraction in the superficial layer was thought to exist only in the ideal or theoretical condition like FE model, the geometry of the stationary contact condition in this study resulted in minimizing of the permeability of the superficial tangential layer. From the precise experimental study, the lubrication mode appeared to enter in the boundary lubrication mode in the sliding speed at less than 1 mm/s in a compressed condition [57], where the equilibrium friction coefficient in bovine synovial fluid (BSF) was considerably smaller than that in phosphate buffered saline (PBS). While the protein constituents in a lubricant were entrapped in

the cartilage surface, it was thought that the superficial tangential layer in their experiment would be compressed so much. Then, the surface permeability was almost minimized so as to recover the friction mode into the mixed lubrication mode along with the increased viscosity by the boosting mechanism [58]. So, the necessity of the tight control of the sliding condition for the frictional experiment of the articular cartilage arised [57]. By a theoretical study, the lubricating squeeze-film in the contact of articular cartilage was predicted to be quickly depleted and worn out in the absence of the characteristic properties of the superficial tangential layer [59]. In spite of stiffening by the fiber reinforcement of the superficial layer in our study, the fiber did not stretch in the tangential direction in the stationary sliding condition, by the geometrical shape shown in Fig. 2(a). The following distribution of the fluid pressure and the field parameters of the solid phase did not show distinct differences over the calculation time between the models. It was thought that the shape of the specimen or the contact geometry would affect the resultant frictional behavior in both the FE analysis and the experimental study. A small radius of the cartilage sample might reduce the effect of fiber reinforced biphasic compression in the study of boundary lubrication.

Beside little difference in the stationary contact condition, the migrating contact condition showed the considerable difference between the models particularly after 100 s. By the cylindrical indentation geometry of the migrating contact condition, stretching of the matrix occurs mainly in the contact area. As shown in Fig. 4, the STZ model started sliding with a little smaller value of friction coefficient than that of the standard model, which implied that the startup friction was smaller in the STZ model. The difference at the immediately after loading would be caused by the simple mechanism. The strengthening of the tangential fiber reinforcement in the superficial layer restricted the horizontal stretch of the tissue at the first indentation, where the interstitial fluid pressurization was promoted by the common manner of the fiber-reinforced biphasic compression. In the parametric study in Fig. 5, the more stiffness of the tangential reinforcement resulted in the less friction coefficient at the starting. The collagen reinforcement in tensile direction is well effective to enhance the interstitial fluid pressurization mainly in dynamic conditions [45,50]. After starting sliding, the friction coefficient of the standard model gradually increased and reached to 0.04 after 100 s sliding, while the STZ model maintained the low friction coefficient. As for the migrating contact condition, the Peclet number $Pe = Va/H_A k$ was one of the indicators for maintaining the fluid load support [60,61], where V is the sliding velocity, a the contact length, H_A the aggregate modulus and k the permeability. As seen in Fig. 8, the contact length did not show an apparent difference between the standard and the STZ model even in the period at 100 s after sliding. The STZ modification of the permeability as the initial value, listed in Table 2, was not so responsible for altering the Peclet number to change the condition drastically. This situation was briefly recognized that the friction coefficient just after starting sliding did not differ between the models.

It was essential to construe what happened in the middle term of the sliding, where the friction coefficient of the STZ model sustained within a smaller value or shortly decreased at 100 s after starting sliding. The first difference of the internal field output was seen in Mises stress formation just beneath of the sliding cylindrical indenter in Fig. 8. At 100 s after sliding, the distinct low-stress layer was observed in the surface zone of the STZ model, which directly meant that the fluid pressure was higher than that of the standard model. Although the difference in the pore pressure distribution was not clearly visualized by the contour plot in absolute value, the length of the high-pressure region in the superficial layer of the STZ model in Fig. 9 was a little wider than that of the standard model. It was notable that the negative pressure region was appeared around the indenter just adjacent to the high-pressure region by the fluid pressurization. Also, the negative pressure was observed in front of the sliding indenter in the STZ model. This situation would be generated by the stiff superficial collagen, which pulled the surface around the indenter and stretched the matrix. The negative pressure in the non-contacting surface leads the drawing of the fluid into the matrix. The re-swelling from the surface is thought to be effective not only for sustaining the fluid load support as a long-term potential but also for directly promoting fluid pressure because the local fluid proportion of the superficial layer especially in front of the indenter would immediately enhance the fluid pressure in the contact area. In the Fig. 10, the flow velocity in the superficial layer of the STZ model was slower than that of the standard model especially in the frontal surface of the indenter while the difference of the pressure gradient was not so obvious between the models seen in Fig. 9. On the one hand the fluid pressure was kept at a high level; on the other hand the fluid did not flow enough to comply the pressure gradient. The reason might be found the volumetric fraction of the fluid phase in Fig. 11. The fluid fraction was reduced in the superficial layer, in which the value decreased to 71%. For example, the 71% of volumetric fluid proportion is equal to 2.45 of the void ratio, and the volumetric aggregation of the solid phase reaches up to 31%. In this condition, the permeability is reduced to 1/12.6, which derives from the material property constant for the compaction effect on permeability M, as presented in Table 1.

The selective decreasement of the permeability in the superficial layer would cause the almost contradictory situation, which were the coexistence of the high fluid pressure and the sub-stationary flow. The interstitial fluid in the superficial layer was exposed to the steep gradient of the fluid pressure in the both the frontal and the behind edge of the contact area. It was thought that the selective decrease of the fluid fraction in superficial layer was caused by the reciprocal motion, which raised this situation repetitively. The low permeability layer sealed the fluid flow at the surface but transmits the fluid pressure efficiently because of its thinness. Although this situation might not be suitable for introducing the law of similarity, the Peclet number was increased locally more than 10 times by the decrease of the permeability at the contacting surface. By a certain increase of the Peclet number, the

frictional performance improves in the fluid load support, which results in the lower friction coefficient. Even though this phenomenon might also develop in the standard model as long as we referred to the contour plots in Fig. 11, the degree of the phenomenon was much significant in the STZ model. As the frictional response of the "Fiber model" in Fig. 4 was similar to the STZ model, the "Fiber model" also organized the low permeability layer in the surface. So, it would be appropriate to note that the low permeability layer was promoted by the stiffening the tangential superficial reinforcement. One of the scenarios to induce this situation was thought to be the following thing. While the superficial layer of the standard model was allowed to stretch in the tangential direction in the loadings of the cylindrical indenter, that of the STZ model was restricted because of the strengthening of the tangential fiber stiffness. In this condition, there was no way except for the tissue aggregating its volume vertically by exuding the fluid mainly from the frontal and the behind edge of the contact area. As a result, the excessive low permeability layer was dynamically organized in the superficial zone.

Meantime, the primary functionality of the superficial tangential reinforcement by the collagen network would be the enhancement of the interstitial fluid pressure in the dynamic condition, as the homogeneous isotropic fiber reinforcement also promoted the fluid pressure considerably [45,49]. The surface fissures could occur in the contact center of a flat surface indenter with the state of "tire burst" [62], which might be explained by the interstitial fluid pressure. The removal of the superficial layer resulted in the increase of the tangential crimping pattern in the deeper zone [63]. The functionality of the superficial tangential layer focused on the permeability was also reported in the past. The removal of the superficial layer significantly reduced the dynamic aggregate modulus even in the confined compression, where the significant lower permeability in the superficial region was discussed as the role of the superficial layer in the compressed state [64]. Recently, the 1-dimensional FE analysis including the depth-dependent compressive modulus of the solid phase and strain-dependent permeability indicated the considerable reduction of the surface permeability by 88% in 0.2 MPa stress and the following removal of the surface zone increased tissue deformation [65]. It was reasonable that the considerable reduction of the surface permeability with the compaction effect would be associated with the large compressive deformation deriving from the small compressive modulus of the surface. They remarked new insights into the role of the superficial zone on the mechanical behavior of artificial cartilage. The permeability change in the compressive condition [66] was also examined in the research field of composite material with the relation between the fabric density changing with the compaction and the permeability [67,68]. The compaction of the composite matrix drastically reduced the permeability, and the nonlinear property of the strain-dependent permeability would cause the complex behavior. According to these reports, it seems that the scenario postulating the sequence for organizing the low permeability layer in this study was not an impossible thing.

The Peclet number as the initial bulk property in this study was of 86, which was a lower limit to maintain the enough performance of the biphasic lubrication in the migrating contact sliding [60]. The sliding speed of the stationary contact condition was also 2 mm/s, which was thought to be just out region of the boundary lubrication mode [57]. And, the stroke length was selected as 4 mm while the contact length was about 2 mm. Although we selected the sliding configuration as a little severe condition for both the migrating and the stationary contact, more various sliding conditions should be examined especially on the ratio of the stroke length to the contact length for the effect on the long term sliding [44,69]. The contact and sliding condition closed within a laboratory conditions as a means of simplification. Of course, more physiological loading condition should be examined for the further implication along with experimental studies. We have to note that the "Standard model" and "Aniso. perm. model" in Fig. 4 showed some reduction of the friction coefficient after 200 s. If more long term sliding was carried out, the friction coefficient might continue reducing while the friction coefficient of the "STZ model" was gradually increasing after 200 s. In this situation, the friction coefficients of these two conditions might be inverted in its position. At the present state, authors could not have identified the reason why the reduction in the friction coefficient of the "Standard model" appeared. We should continue observing this peculiar behavior with more careful observations of the internal behavior in the model. Once we could figure out the reason, it would bring some worthful insight not only for the recognition of synovial articular cartilage but also the development of artificial cartilage system. The extra parametric study of the "8.0 times model" showed the interesting result as shown in Fig. 5. Since the tangential stiffness of the tissue including the superficial layer was experimentally 6 times higher than that prepared from the middle zone [33], the "8.0 times model" was worth accepting as an eventual condition. In the parametric study on the strengthening of the fiber stiffness, the permeability in the superficial tangential layer was jointly changed with the stiffness. In this study, we assumed that the strengthen of the superficial collagen causes the increase of the permeability in fiber direction from the structural viewpoint [40]. This methodology might cause some obscure things from an engineering standpoint because the effects of the stiffness and the increased permeability were mixed in Fig. 5. Although the contribution of each element was partly discussed in the Fig. 4, we had better keep the parameter constant in changing the other parameter in a further investigation. This deliberate attempt might lead to clarify each potential of the element and also to find the synergistic effect in different stiffnesses. For saving computational time and for an unproblematic implementation of the sliding conditions, we admitted the 2-dimensional modeling, which might conceal the realistic situation. Although the split-line pattern did not directly relate to the spatial pattern of the contact and pore pressure in a physiological 3D model [70], our model is thought to represent the phenomena in the split-line direction. Another notable property was the compression induced anisotropy of the

permeability [39] while the anisotropic diffusional property of articular cartilage in compression was explained by several compaction stages of the matrix construction [71]. Then, Fujie et al. studied the prospective functionality of the compression induced anisotropy on the permeability in the startup and the dynamic friction [42]. We should also discuss this particular property on the permeability by incorporating it into the model with the consideration of the thickness of the superficial tangential layer. In the regenerative cartilage tissue, a small self-assembled collagen fragment aggregated around the cell and formed the interconnective organization under a cyclic compressive cultivation [72]. Since the collagen network of newborn cartilage did not show the distinct depth-wise structure, the characteristic fibrous structure of articular cartilage was thought to be a result of the remodeling to the loading condition during maturation with its thickness being decreased [55,73]. In this consideration, the split-line pattern might be organized by the remodeling as a loading response. The findings in this study would provide biomechanical illustrations for the organization of articular cartilage. From an engineering perspective, the functional mechanism of articular cartilage as a load bearing system would also offer beneficial insights for the advances of tribology in general [74]. It is thought that the development of the artificial cartilage system inspired by these phenomena is one of the experimental verification ways and also the certain objective of this study.

5. Conclusion

The stiffening by the tangential fiber reinforcement of superficial layer of articular cartilage showed the significant reduction in friction in the migrating contact sliding. The thin low permeability layer was formed in the contact length of the reciprocal sliding indenter. The thin low permeable layer enabled the contradictory phenomenon of both the high fluid pressurization in the surface and the low fluid flow. The stiffening of the fiber reinforcement of the superficial layer promoted the formation of the low permeability layer. While the fiber reinforcement of biphasic material was well efficient to enhance the interstitial fluid pressurization in a short term, the compaction effect on the permeability would involve a considerable complex situation in long term migrating contact sliding.

Acknowledgments

Financial support was given by the Grant-in-Aid for Specially Promoted Research of Japan Society for the Promotion of Science: KAKENHI (23000011).

References

[1] A. Maroudas, P. Bullough, Permeability of articular cartilage, Nature 219 (1968) 1260–1261.
[2] W.S. vanden Berg-Foels, L. Scipioni, C. Huynh, A. Wen, Helium ion microscopy for high-resolution visualization of the articular cartilage collagen network, J. Microsc. 246 (2012) 168–176.
[3] V.C. Mow, A. Ratcliffe, A.R. Poole, Cartilage and diarthrodial joints as paradigms for hierarchical materials and structure, Biomaterials 13 (1992) 67–97.
[4] R.M. Schinagl, D. Gurskis, A.C. Chen, R.L. Sah, Depth-dependent confined compression modulus of full-thickness bovine articular cartilage, J. Orthop. Res. 15 (1997) 499–506.
[5] O.K. Erne, J.B. Reid, L.W. Ehmke, M.B. Sommers, S.M. Madey, M. Bottlang, Depth-dependent strain of patellofemoral articular cartilage in unconfined compression, J. Biomech. 38 (2005) 667–672.
[6] J.S. Jurvelin, M.D. Bushmann, E.B. Hunziker, Mechanical anisotropy of the human knee articular cartilage in compression, Proc. Inst. Mech. Eng. Part H: J. Eng. Med. 217 (2003) 215–219.
[7] C.C.-B. Wang, N.O. Chahine, C.T. Hung, G.A. Ateshian, Optical determination of anisotropic material properties of bovine articular cartilage in compression, J. Biomech. 36 (2003) 339–353.
[8] C.-Y. Huang, M.A. Soltz, M. Kopacz, V.C. Mow, G.A. Ateshian, Experimental verification of the roles of intrinsic matrix viscoelasticity and tension–compression nonlinearity in the biphasic response of cartilage, ASME J. Biomech. Eng. 125 (2003) 84–93.
[9] N.O. Chahine, C.C.-B. Wang, C.T. Hung, G.A. Ateshian, Anisotropic strain-dependent material properties of bovine articular cartilage in the transitional range from tension to compression, J. Biomech. 37 (2004) 1251–1261.
[10] T. Murakami, H. Higaki, Y. Sawae, N. Ohtsuki, S. Moriyama, Y. Nakanishi, Adaptive multimode lubrication in natural synovial joints and artificial joints, Proc. Inst. Mech. Eng. Part H: J. Eng. Med. 212 (1998) 23–35.
[11] J. Klein, Molecular mechanisms of synovial joint lubrication, Proc. Inst. Mech. Eng. Part J: J. Eng. Tribol. 220 (2006) 691–710.
[12] T. Sasada, Surface gel hydration lubrication in animal joints, J. Jpn. Soc. Tribol. 52 (2007) 573–578.
[13] T. Murakami, Y. Sawae, K. Nakashima, S. Yarimitsu, T. Sato, Micro- and nanoscopic biotribological behaviours in natural synovial joints and artificial joints, Proc. Inst. Mech. Eng. Part H: J. Eng. Med. 221 (2007) 237–245.
[14] R. Nansai, T. Suzuki, K. Shimomura, W. Ando, N. Nakamura, H. Fujie, Surface morphology and stiffness of cartilage-like tissue repaired with scaffold-free tissue engineered construct, J. Biomech. Sci. Eng. 6 (2011) 40–48.
[15] S. Graindorge, W. Ferrandez, E. Ingham, Z. Jin, P. Twigg, J. Fisher, The role of the surface amorphous layer of articular cartilage in joint lubrication, Proc. Inst. Mech. Eng. Part H: J. Eng. Med. 220 (2006) 597–607.
[16] J. Katta, Z. Jin, E. Ingham, J. Fisher, Biotribology of articular cartilage—a review of the recent advances, Med. Eng. Phys. 30 (2008) 1349–1363.
[17] T. Murakami, K. Nakashima, Y. Sawae, N. Sakai, S. Yarimitsu, N. Hosoda, Roles of adsorbed film and gel layer in hydration lubrication for articular cartilage, Proc. Inst. Mech. Eng. Part H: J. Eng. Med. 223 (2009) 287–295.
[18] S. Yarimitsu, K. Nakashima, Y. Sawae, T. Murakami, Influences of lubricant composition of forming boundary film composed of synovia constituents, Tribol. Int. 42 (2009) 1615–1623.
[19] T. Murakami, K. Nakashima, S. Yarimitsu, Y. Sawae, N. Sakai, Effectiveness of adsorbed film and gel layer in hydration lubrication as adaptive multimode lubrication mechanism for articular cartrilage, Proc. Inst. Mech. Eng. Part J: J. Eng. Tribol. (2011) 1174–1185.
[20] V.C. Mow, S.C. Kuei, W.M. Lai, C.G. Armstrong, Biphasic creep and stress relaxation of articular cartilage in compression: theory and experiments, J. Biomech. Eng. 102 (1980) 73–84.
[21] G.A. Ateshian, The role of interstitial fluid pressurization in articular cartilage lubrication, J. Biomech. 42 (2009) 1163–1176.
[22] G.A. Ateshian, A theoretical formulation for boundary friction in articular cartilage, J. Biomech. Eng. 119 (1997) 81–86.
[23] S. Park, R. Krishnan, S.B. Nicoll, G.A. Ateshian, Cartilage interstitial fluid load support in unconfined compression, J. Biomech. 36 (2003) 1785–1796.

[24] R. Krishnan, M. Kopacz, G.A. Ateshian, Experimental verification of the role of interstitial fluid pressurization in cartilage lubrication, J. Orthop. Res. 22 (2004) 565–570.
[25] M.L. Wang, Z.X. Peng, Wear inhumanknees, Biosurf. Biottibol. 1 (2015) 98–112.
[26] T. McCormack, J.M. Mansour, Reduction in tensile strength of cartilage precedes surface damage under repeated compressive loading in vitro, J. Biomech. 31 (1998) 55–61.
[27] M. Thibault, A.R. Poole, M.D. Buschmann, Cyclic compression of cartilage/bone explants in vitro leads to physical weakening, mechanical breakdown of collagen and release of matrix fragments, J. Orthop. Res. 20 (2002) 1265–1273.
[28] B. Rolauffs, C. Muehleman, J. Li, B. Kurs, K.E. Kuettner, E. Frank, A.J. Grodzinsky, Vulnerability of the superficial zone of immature articular cartilage to compressive injury, Arthritis Rheum. 62 (2010) 3016–3027.
[29] A. Thambyah, N. Broom, Micro-anatomical response of cartilage-on-bone to compression: mechanisms of deformation within and beyond the directly loaded matrix, J. Anat. 209 (2006) 611–622.
[30] A. Thambyan, N. Broom, On how degeneration influences load-bearing in the cartilage–bone system: a microstructural and micromechanical study, Osteoarthr. Cartil. 15 (2007) 1410–1423.
[31] S.L. Bevill, A. Thambyah, N.D. Broom, New insights into the role of the superficial tangential zone in influencing the microstructural response of articular cartilage to compression, Osteoarthr. Cartil. 18 (2010) 1310–1318.
[32] R.K. Korhonen, M. Wong, J. Arokoski, R. Lindgren, H.J. Helminen, E. B. Hunziker, J.S. Jurvelin, Importance of the superficial tissue layer for the indentation stiffness of articular cartilage, Med. Eng. Phys. 23 (2004) 99–108.
[33] M. Charlebois, M.D. McKee, M.D. Buschmann, Nonlinear tensile properties of bovine articular cartilage and their variation with age and depth, J. Biomech. Eng. 126 (2004) 129–137.
[34] W. Wilson, C.C. van Donkelaar, B. van Rietbergen, K. Ito, R. Huiskes, Stresses in the local collagen network of articular cartilage: a poroviscoelastic fibril-reinforced finite element study, J. Biomech. 37 (2004) 357–366.
[35] S. Federico, A. Grillo, G.L. Rosa, G. Giaquinta, W. Herzog, A transversely isotropic, transversely homogeneous microstructural–statistical model of articular cartilage, J. Biomech. 38 (2005) 2008–2018.
[36] P. Julkunen, P. Kiviranta, W. Wilson, J.S. Jurvelin, R.K. Korhonen, Characterization of articular cartilage by combining microscopic analysis with a fibril-reinforced finite-element model, J. Biomech. 40 (2007) 1862–1870.
[37] R.K. Krishnan, S. Park, F. Eckstein, G.A. Ateshian, Inhomogeneous cartilage properties enhance superficial interstitial fluid support and frictional properties, but do not provide a homogeneous state of stress, J. Biomech. Eng. 125 (2003) 569–577.
[38] H.A. Leddy, F. Guilak, Site-specific effects of compression on macromolecular diffusion in articular cartilage, Biophys. J. 95 (2008) 4890–4895.
[39] B. Reynaud, T.M. Quinn, Anisotropic hydraulic permeability in compressed articular cartilage, J. Biomech. 39 (2006) 131–137.
[40] S. Federico, W. Herzog, On the anisotropy and inhomogeneity of permeability in articular cartilage, Biomech. Model. Mechanobiol. (2008) 367–378.
[41] Y. Dabiri, L.P. Li, Influences of the depth-dependent material inhomogeneity of articular cartilage on the fluid pressurization in the human knee, Med. Eng. Phys. 35 (2013) 1591–1598.
[42] H. Fujie, K. Imade, Effects of low tangential permeability in the superficial layer on the frictional property of articular cartilage, Biosurf. Biotribol. 1 (2015) 124–129.
[43] N. Sakai, Y. Hagihara, C. Hashimoto, M. Komori, Y. Sawae, T. Murakami, An estimation of mechanical properties of articular cartilage for biphasic finite element analyses, J. Biomech. Sci. Eng. 10 (2015) 15–00228, http://dx.doi.org/10.1299/jbse.15-00228.
[44] S.S. Pawaskar, Z.M. Jin, J. Fisher, Modelling of fluid support inside articular cartilage during sliding, Proc. Inst. Mech. Eng. Part J: J. Eng. Tribol. (2007) 165–174.
[45] N. Sakai, Y. Hagihara, T. Furusawa, N. Hosoda, Y. Sawae, T. Murakami, Analysis of biphasic lubrication of articular cartilage loaded by cylindrical indenter, Tribol. Int. 46 (2012) 225–236.
[46] N. Hosoda, N. Sakai, Y. Sawae, T. Murakami, Depth-dependence and time-dependence in mechanical behavior of articular cartilage in unconfined compression test under constant total deformation, J. Biomech. Sci. Eng. 3 (2008) 209–220.
[47] S. Graindorge, W. Ferrandez, Z. Jin, E. Ingham, C. Grant, P. Twigg, J. Fisher, Biphasic surface amorphous layer lubrication of articular cartilage, Med. Eng. Phys. 27 (2005) 836–844.
[48] S. Graindorge, W. Ferrandez, Z.-M. Jin, E. Ingham, J. Fisher, The natural synovial joint: a finite element investigation of biphasic surface amorphous layer lubrication under dynamic loading conditions, Proc. Inst. Mech. Eng. Part H: J. Eng. Med. 220 (2006) 671–681.
[49] L.P. Li, J. Soulhat, M.D. Buschmann, A. Shirazi-Adl, Nonlinear analysis of cartilage in unconfined ramp compression using a fibril reinforced poroelastic model, Clin. Biomech. 14 (1999) 673–682.
[50] R. Shirazi, A. Shirazi-Adl, Deep vertical collagen fibrils play a significant role in mechanics of articular cartilage, J. Orthop. Res. 26 (2008) 608–615.
[51] L.P. Li, R.K. Korhonen, J. Iivarinen, J.S. Jurverin, W. Herzog, Fluid pressure driven fibril reinforcement in creep and relaxation tests of articular cartilage, Med. Eng. Phys. 30 (2008) 182–189.
[52] H.A. Leddy, M.A. Haider, G. Guilak, Diffusional anisotropy in collagenous tissues: fluorescence imaging of continuous point photobleaching, Biophys. J. 91 (2006) 311–316.
[53] F. Hontoir, P. Clegg, J.F. Nisolle, S. Tew, J.M. Vandeweerd, Magnetic resonance compositional imaging of articular cartilage: What can we expect in veterinary medicine?, Vet. J. 205 (2015) 11–20.
[54] K.B. Gu, L.P. Li, A human knee joint model considering fluid pressure and fiber orientation in cartilages and menisci, Med. Eng. Phys. 33 (2011) 497–503.
[55] P. Julkunen, W. Wilson, H. Isaksson, J.S. Jurvelin, W. Herzog, R. K. Korhonen, A review of the combination of experimental measurements and fibril-reinforced modeling for investigation of articular cartilage and chondrocyte response to loading, Comput. Math. Methods Med. (2013) 23, http://dx.doi.org/10.1155/2013/326150.
[56] S. Federico, W. Herzog, On the permeability of fibre-reinforced porous materials, Int. J. Solids Struct. 45 (2008) 2160–2172.
[57] J.P. Gleghorn, L.J. Bonassar, Lubrication mode analysis of articular cartilage using Stribeck surfaces, J. Biomech. 41 (2008) 1910–1918.
[58] P.S. Walker, D. Dowson, M.D. Longfield, V. Wright, "Boosted lubrication" in synovial joints by fluid entrapment and enrichment, Ann. Rheum. Dis. 27 (1968) 512–520.
[59] M. Hlaváček, Squeeze-film lubrication of the human ankle joint with synovial fluid filtrated by articular cartilage with the superficial zone worn out, J. Biomech. 33 (2000) 1415–1422.
[60] M. Caligaris, G.A. Ateshian, Effects of sustained interstitial fluid pressurization under migrating contact area, and boundary lubrication by synovial fluid, on cartilage friction, Osteoarthr. Cartil. 16 (2008) 1220–1227.
[61] A.C. Moore, D.L. Burris, An analytical model to predict interstitial lubrication of cartilage in migrating contact areas, J. Biomech. 47 (2014) 148–153.
[62] A.J. Kerin, M.R. Wisnom, M.A. Adams, The compressive strength of articular cartilage, Proc. Inst. Mech. Eng. Part H: J. Eng. Med. 212 (1998) 273–280.
[63] C. Glaser, R. Puts, Functional anatomy of articular cartilage under compressive loading, quantitative aspects of global, local and zonal reactions of the collagenous network with respect to the surface integrity, Osteoarthr. Cartil. 10 (2002) 83–99.
[64] A.R. Gannon, T. Nagel, D.J. Kelly, The role of the superficial region in determining the dynamic properties of articular cartilage, Osteoarthr. Cartil. 20 (2012) 1417–1425.

[65] H. Guo, S.A. Maher, P.A. Torzilli, A biphasic finite element study on the role of the articular cartilage superficial zone in confined compression, J. Biomech. 48 (2015) 166–170.
[66] W.Y. Gu, H. Yao, C.Y. Huang, H.S. Cheung, New insight into deformation-dependent hydraulic permeability of gels and cartilage, and dynamic behavior of agarose gels in confined compression, J. Biomech. 36 (2003) 593–598.
[67] M.J. Buntain, S. Bickerton, Compression flow permeability measurement: a continuous technique, Compos. Part A 34 (2003) 445–457.
[68] S. Comas-Cardona, C. Binetruy, P. Krawczak, Unidirectional compression of fibre reinforcements. Part 2: a continuous permeability tensor measurement, Compos. Sci. Technol. 67 (2007) 638–645.
[69] M.A. Accardi, D. Dini, P.M. Cann, Experimental and numerical investigation of the behaviour of articular cartilage under shear loading —interstitial fluid pressurisation and lubrication mechanisms, Tribol. Int. 44 (2011) 565–578.
[70] M.E. Mononen, M.T. Mikkola, P. Julkunen, R. Ojala, M.T. Nieminen, J.S. Jurvelin, R.K. Korhonen, Effect of superficial collagen patterns and fibrillation of femoral articular cartilage on knee joint mechanics—a 3D finite element analysis, J. Biomech. 45 (2012) 579–587.
[71] G.W. Greene, B. Zappone, B. Zhao, O. Söderman, D. Topgaard, G. Rata, J.N. Israelachvili, Changes in pore morphology and fluid transport in compressed articular cartilage and the implications for joint lubrication, Biomaterials 29 (2008) 4455–4462.
[72] S. Omata, Y. Sawae, T. Murakami, Tissue development and mechanical property in the regenerated-cartilage tissue, in: L. Ceccherini-Nelli, B. Matteoli (Eds.), Biomedical Tissue Culture, InTech, Croatia, 2012, pp. 133–150.
[73] W. Gründer, MRI assessment of cartilage ultrastructure, NMR Biomed. 19 (2006) 855–876.
[74] Z.R. Zhou, Z.M. Jin, Biotribology: recent progresses and future perspectives, Biosurf. Biotribol. 1 (2015) 3–24.